Journal of Statistical Physics, Vol. 44, Nos. 5/6, 1986

Geometry of Random Sequential Adsorption

Einar L. Hinrichsen,[1] Jens Feder,[1] and Torstein Jøssang[1]

Received November 18, 1985; final March 24, 1986

By sequentially adding line segments to a line or disks to a surface at random positions without overlaps, we obtain configurations of the one- and two-dimensional random sequential adsorption (RSA) problem. We have simulated the one- and two-dimensional problem with periodic boundary condition. The one-dimensional simulations are compared with the exact analytical solutions to give an estimate of the accuracy of the simulation. In two dimensions the geometrical properties of the RSA configuration are discussed and in addition known results of the RSA process are reproduced. Various statistical distributions of the Voronoi–Dirichlet (VD) network corresponding to the RSA disk configuration are analyzed. In order to characterize pores in the RSA configuration, we introduce circular holes. There is a direct correspondence between vertices of the VD network and these holes, and also between direct/indirect geometrical neighbors and these holes. The hole size distribution is found to be a parabola. We also find general relations that connect the asymptotic behavior of the surface coverage, the correlation function, and the hole size distribution.

KEY WORDS: Random sequential adsorption; random disk packing; correlations; pore size distribution; Voronoi–Dirichlet network.

1. INTRODUCTION

A number of problems arising in chemistry, biology, and physics involve processes that occur sequentially and which are essentially irreversible over typical observation times. The random sequential adsorption (RSA) model is a random packing model which has attracted a lot of attention because of its many applications to such problems. The model has been used to describe oxidation of polymers,[1] particles in a biological membrane,[2] spatial patterns in ecological systems[3] and adsorption of proteins on solid surfaces.[4] The RSA model was also introduced to describe the geometry of the fluid phase of a hard sphere system. But as Widom[5] pointed out, the

[1] Department of Physics, University of Oslo, Blindern, 0316 Oslo 3, Norway.

0022-4715/86/0900-0793$05.00/0

822/44/5-6-6

RSA configuration and the configuration characteristic of a hard sphere system in thermodynamic equilibrium at the same density, are fundamentally different.

In spite of the importance of getting a good geometrical description of the RSA configuration, most of the work done on the two-dimensional RSA problem have been dealing with the problem of finding the value of the surface coverage θ_2 (the fraction of area covered by disks) at the jamming limit. Very little has been done on characterizing the geometrical properties of the RSA configuration. The geometrical aspect of the problem is difficult, as may be appreciated when the complicated shape and topology of the area not occupied by disks are considered. Good descriptions of the geometrical properties of random disk packings are needed in comparing various models with experiments. Also, as a result of the recent interest in porous and other random media, better concepts for describing random geometries are needed. In porous media the problem of giving precise definition of pore sizes, shapes, and their connectivity properties is related to the problem of how geometrical properties influence the transport properties of fluid in the pores.

The basic model of random sequential adsorption in D dimensions is

- The objects are placed at random in a D-dimensional volume (surface in two dimensions) in a sequential order.
- If the last placed object overlaps any other objects, it is removed at once.
- Once an object has been placed, its position is permanently fixed.
- When no more objects can be placed without overlapping those already present, the jamming limit has been reached and the process stops.

The objects adsorbed are normally hyperspheres or hypercubes, but can in principle be of any geometrical shape. Because of the perfect memory of the RSA process, it is extremely non-Markovian, even though each step is completely random. As a result, the RSA configuration has some very interesting and unusual geometrical features.

If the objects adsorbed are spheres with equal diameter d, the radial distribution function $G(r)$ has a logarithmic divergence at contact in any dimension D[6–8]

$$G(r) \xrightarrow[r \to d]{} \ln(r-d) \tag{1}$$

Also, the asymptotic behavior of the coverage θ_D in D dimensions for the RSA process of equal spheres is[6–8]

$$\theta_D(\infty) - \theta_D(\tau) \sim \tau^{-1/D} \tag{2}$$

instead of a τ^{-1} dependence that one naively would have expected.[6] Here τ is a time parameter proportional to the number of attempts made to place disks.

The one-dimensional case, also known as the parking problem, is exactly solvable.[1,5,9-11] The limiting coverage at saturation is $\theta_1(\infty) = 0.747597\ldots$.[12] In two (and higher) dimensions there are two obvious generalizations of the one-dimensional case, the adsorption of aligned squares, or the adsorption of disks (hyperspheres) onto a surface (volume). The placing of aligned squares and disks on a surface give different results for the coverage.[6,13,14] Also the saturation of $\theta_2(\tau)$ and the singularity of $G(r)$ are different.[8] The coverage for aligned two-dimensional squares is found to be $\theta(\infty) = 0.563 \pm 0.002$,[6] while the coverage of two-dimensional disks is found to be $\theta_2(\infty) = 0.5473 \pm 0.0009$ by Tanemura[15] and $\theta_2(\infty) = 0.547 \pm 0.002$ by Feder.[6] These values for the surface coverage and the asymptotic behavior of $G(r)$ and $\theta_D(\tau)$ in eqs. (1) and (2) are the only geometrical results known for the two-dimensional RSA problem.

In this paper we report results obtained by simulating the RSA of disks in two dimensions. All known properties of the RSA problem are verified. In addition we discuss the geometrical properties in great detail. We discuss various statistical distributions of the Voronoi–Dirichlet (VD) network of the RSA configuration. Bernal and Finney[16-18] have long advocated that the statistical properties of the VD polygons should be the cornerstone in a description of statistical geometry.

In order to characterize the pores in the RSA configuration, we introduce *circular holes*. We find a direct correspondence between these holes and the vertices of the VD polygons. The notions of *stable* and *unstable holes* correspond to *direct* and *indirect geometrical neighbors*. The hole size distribution $P(d_h)$ at jamming—where d_h is a hole diameter—is found to be described by a parabola. At the cutoff value, where the hole diameter d_h equals the disk diameter d, $P(d_h = d)$ has approximately the same value in one and two dimensions. We show that the asymptotic form of the correlation function and the coverage can be written as

$$G(r) = -\frac{(D+1)\,T_D}{D2^{D-1}} \frac{1}{\theta_D(\infty)} P(d_h = d) \ln\left(\frac{r}{d} - 1\right) + \cdots \quad (3)$$

and

$$\theta_D(\infty) - \theta_D(\tau) = \frac{T_D}{D} K_D \theta_D(\infty)\, P(d_h = d)\, \tau^{-1/D} + \cdots \quad (4)$$

Here T_D is a topological number defined as the number of vertices per cell in a D-dimensional random VD network. K_D is a geometrical constant. In

one dimension $K_1 = 1$. On the basis of our two-dimensional simulations we find also that $K_2 = 1$. This may be the case for general D. Relation (3) and (4) give connections between the surface saturation, the correlation function, and the hole size distribution function.

This paper is organized as follows: In Section 2 we describe the simulations of the one-dimensional problem. These results are compared with the exact analytical results to test our algorithm and calculation accuracy. In Section 3 we discuss our implementation of the two-dimensional RSA algorithm and present our results for the coverage at the jamming limit where there is no hole big enough for placing another disk on the surface. We also discuss the time-dependent saturation of the coverage implied by this algorithm. In Section 4 we define holes or pores for such configurations, and introduce the size distribution of these holes. The two-particle correlation function and its logarithmic divergence at contact is discussed in Section 5. Finally, in Section 6 we present some statistical results for the Voronoi–Dirichlet polygons of these configurations. A short summary is given in Section 7.

2. THE ONE-DIMENSIONAL RSA PROBLEM

The main purpose of this paper is to study the two-dimensional RSA problem of placing disks on a surface using an algorithm of Feder.[6] Because of the logarithmic divergence of the correlation function at contact one needs to be careful in order to obtain accurate results. Small differences in the algorithms used lead to different estimates of the limiting coverage. Finegold and Donnell[2] used a fine-mesh method where the target area is divided into 1024×1024 small squares. A disk placed on the surface is centered on a small square and the disk is represented by the minimum set of small squares which completely covers its area. In their simulations they used disks with diameter 27.5 times the side of a square and the difference between the surface of a disk and the array of squares representing a disk was less than 1.5%. In spite of this small error, their results are approximately 10% below the results obtained by Tanemura[15] and Feder.[6] Tory, Jodrey, and Pickard[14] have investigated the sensitivity of the results to the approximation made in this fine-mesh method.

Several pseudo random number generators are known to result in statistical dependencies that are very difficult to control. In addition, the computer rounding errors create a situation where the results may depend on the details of the algorithm used. It is therefore useful to repeat previous simulations on different computers (here we use a ND-500, whereas our first two-dimensional simulations[6] were made using a VAX-780 system). The random number generator in these simulations is a Fortran version of

the IBM assembler routine RNDM2 in CERN's program library. The generator is a combined multiplicative congruential generator and a shift register generator designed to give a cycle of approximately $5 \cdot 10^{18}$ numbers and with nearly optimal lattice structure in two to five dimensions. The one-dimensional RSA problem, because of the analytical results available, provides a good test for the adequacy of the random number generator used.

In one dimension the time-dependent coverage $\theta_1(\tau)$ is[1]

$$\theta_1(\tau) = \int_0^\tau du \exp\left[-2 \int_0^u dv \frac{1}{v} (1 - e^{-v}) \right] \tag{5}$$

τ is time given in units of $L/d\lambda$ where λ is the rate at which attempts are made to place line segments of length d on a line of length L. When $\tau \to \infty$, $\theta_1(\tau)$ has the following asymptotic behavior

$$\theta_1(\tau) = \theta_1(\infty) - \frac{e^{-2\gamma}}{\tau} + \cdots \tag{6}$$

where $\gamma = 0.5772...$ is the Euler's constant. $\theta_1(\infty)$ is the coverage at the jamming limit; $\theta_1(\infty) = 0.747597....$

A hole in a configuration is the space between two adjacent line segments. The probability density function $p(x)$ for finding holes with size between x and $x + dx$ at jamming was shown by Mackenzie[10] to be

$$p(x) = \frac{2}{\theta_1(\infty)} \frac{1}{d} \int_0^\infty du\, u e^{-ux} \exp\left[-2 \int_0^u dv \frac{1}{v} (1 - e^{-v}) \right] \tag{7}$$

This distribution diverges as $x \to 0$

$$p(x) = -\frac{2}{\theta_1(\infty)} \frac{1}{d} e^{-2\gamma} \ln \frac{x}{d} + \cdots \tag{8}$$

The reason for this divergence is explained in Appendix A. When $x = d$ the distribution has the value

$$p(x = d) = \frac{1}{\theta_1(\infty)} \frac{1}{d} e^{-2\gamma} = d^{-1} \cdot 0.4217... \tag{9}$$

In our one-dimensional simulations we used a relative line length $d/L = 2 \cdot 10^{-4}$. To generate each configurtion we made 10^8 attempts at placing line segments on a line with periodic boundary conditions. This took approximately 1 CPU hour on our ND-500 computer. We made 18

independent runs, and after 10^8 attempts most of our configurations were jammed. The time-dependent coverage averaged over these 18 runs is plotted in Fig. 1, where we also have plotted the deviation between the simulated points and the theoretical value obtained from eq. (5). The agreement is within our statistical errors. Our result for the coverage at the jamming limit is $\theta_1(\infty) = 0.7477 \pm 0.0023$, in agreement with the exact result.

To test the asymptotic behavior of the line saturation we have plotted $\theta_1(\tau)$ versus $1/\tau$ in Fig. 2. In the same figure we have also plotted the exact asymptote given by eq. (6); $\theta_{as}(\tau) = \theta_1(\infty) - e^{-2\gamma}/\tau$. The convergence to the asymptotic behavior is slow. We find the same slow convergence in our two-dimensional simulations. A least-squares fit of the data points in Fig. 2 for τ^{-1} in the interval (0, 0.2) (or $5 < \tau < \infty$) gave $\theta_1(\tau) = 0.7477 - 0.3136/\tau$ with a standard deviation of $4 \cdot 10^{-6}$ per point. The exact asymptote in Fig. 2 is $\theta_{as}(\tau) = 0.7476 - 0.3152/\tau$. Observe that $\theta_{as}(\tau)$ can be written as

$$\theta_{as}(\tau) = \theta_1(\infty) - d\,\theta_1(\infty)\; p(x = d)\; 1/\tau \tag{10}$$

Such an expression appear to be valid in two (and higher) dimensions.

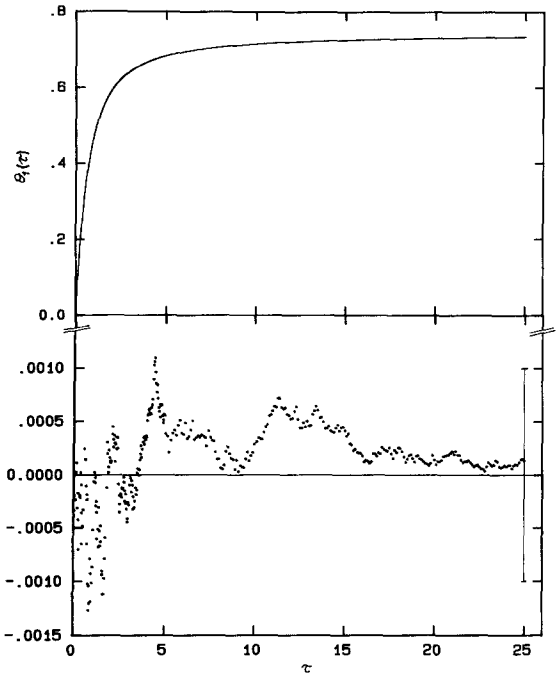

Fig. 1. The top figure is the coverage as a function of time τ averaged over 18 independent runs. The lower figure shows the deviation of the simulated points from the theoretical values. The error bar, shown for comparison, is 1 s.d. obtained at the jamming limit for the 18 runs.

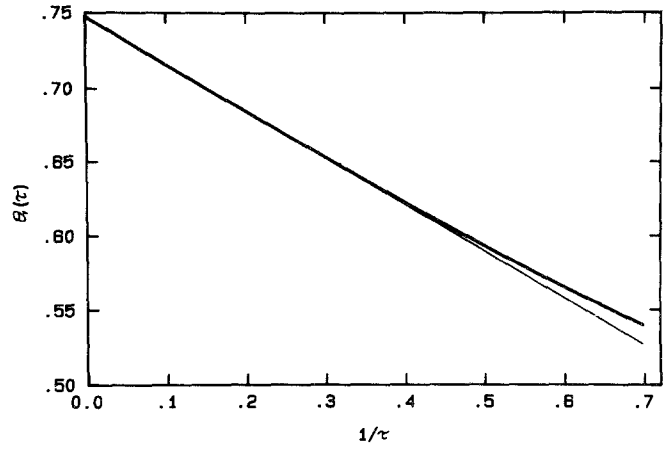

Fig. 2. The asymptotic behavior of the coverage $\theta_1(\tau)$. The straight line is the exact asymptote.

Next consider the hole distribution. In Fig. 3 we have plotted the simulated hole distribution and the theoretical hole distribution $p(x)$ given in eq. (7). The agreement is seen to be good. To test the asymptotic behavior, we also show our simulated points plotted versus $\ln x$ for $x/d < 0.2$ together with the asymptotic result in eq. (8). We have reasonable agreement even though we have bad statistics for really small x. A fit of the

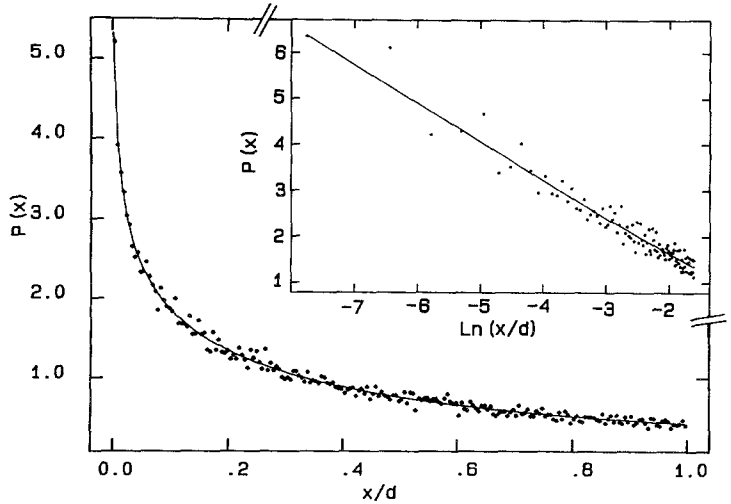

Fig. 3. The main figure is the simulated and exact hole distribution $p(x)$. The insert is the asymptotic behavior for small x. The straight line is the exact asymptote.

simulated points to a straight line for $\ln x/d < -1.6$ gives $p(x) = 0.85d^{-1} \ln x + \cdots$, whereas the exact result of eq. (8) gives $p(x) = 0.8433d^{-1} \ln x + \cdots$.

A general definition of the radial distribution function $G(d+x)$ is given in Sect. 5, but for the one-dimensional case we have

$$\bar{n}G(d+x)2\,dx = \textit{Probability of finding the center of a line segment in dx a distance } (d+x) \textit{ from a given line segment centered at the origin}$$

Here $\bar{n} = \theta_1(\infty)/d$ is the number density of line segments. With this definition $G(d+x)$ is normalized so that $G(d+x) \to 1$ when $x \to \infty$. Since we have one hole on each side of a given line segment this probability must equal $2p(x)\,dx$ for $x < d$, and therefore we find that

$$G(d+x) = \frac{1}{\bar{n}}\,p(x) = \frac{d}{\theta_1(\infty)}\,p(x), \qquad x < d \tag{11}$$

Using eq. (8) we find for small x

$$G(d+x) = -\frac{2}{\theta_1(\infty)^2}\,e^{-2\gamma} \ln \frac{x}{d} + \cdots = -1.128 \ln \frac{x}{d} + \cdots \tag{12}$$

We conclude that our simulations give accurate results in the one-dimensional case, and that the random number generator used is adequate for this type of simulations.

3. THE TWO-DIMENSIONAL RSA CONFIGURATION

In our simulations of the two-dimensional RSA problem of placing disks on a surface we do not make any other approximations than the unavoidable round-off error in the computer. It is too inefficient to search the whole array of earlier placed disks checking for overlap each time a new attempt of placing a disk on the surface is made. Instead we divide the unit square into a grid of small cells. The diagonal of a cell is chosen to be slightly less than the diameter of a disk. With this size of a cell, there is at most one disk center in each cell. We test for overlap by searching through the neighboring cells to see if they are occupied or not. If some of them are occupied, we calculate the distance between the disk centers to check for overlap.

We have made 35 independent simulations of placing disks with relative area $a = 2 \cdot 10^{-4}$ on a unit square with periodic boundary conditions. Each configuration took approximately 3 CPU hours on our

ND-500 computer. To generate each disk configuration we made 10^8 attempts of placing disks on the unit square. At this stage we identified the holes that are large enough to contain disks. By placing disks at random in these holes we obtained the completely jammed configuration. A typical configuration is shown in Fig. 4. In Section 4 we explain how we identify holes that can contain a disk. The average coverage of these jammed configurations is $\theta_2(\infty) = 0.547 \pm 0.003$, corresponding to 2734 ± 13 disks on the surface. This is in agreement with Tanemura[15] and Feder.[6]

To test how sensitive this result is to the relative disk area used, we repeated the simulation for various disk areas. The result is summarized in Table I. We see that the average is insensitive to the disk size but that the fluctuations increase with increasing disk size. The total average of all 115 configurations in the last column gives $\theta_2(\infty) = 0.5471 \pm 0.0051$.

The theoretical result for asymptotic dynamics of the adsorption process (see appendix A)[7,8] is

$$\theta_2(\infty) - \theta_2(\tau) \sim \tau^{-1/2} \tag{13}$$

where τ is time. A time unit is defined as $1/a$ trials of placing disks with area a on the unit square. To make a test of this result we show in Fig. 5 a

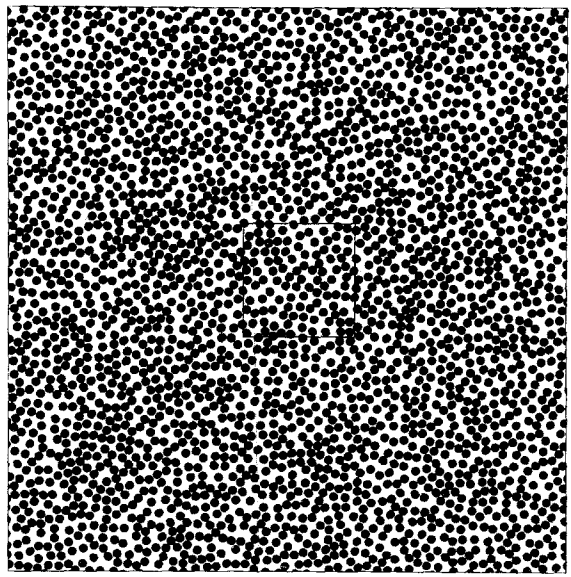

Fig. 4. The figure shows an RSA configuration at the jamming limit. The central square is magnified in Fig. 14.

Table I. The Result of the RSA Simulation for Different Values of the Relative Disk Area a.[a]

a	Coverage
0.01	0.547 ± 0.2
0.008	0.546 ± 0.02
0.006	0.550 ± 0.02
0.004	0.549 ± 0.009
0.002	0.550 ± 0.006
0.001	0.549 ± 0.007
0.0008	0.547 ± 0.006
0.0006	0.547 ± 0.004
0.0004	0.547 ± 0.004
0.0002	0.547 ± 0.003

[a] For each value of a we made 20 independent configurations, except for $a = 0.0002$ where we made 35.

plot of the coverage averaged over the 35 configurations[2] with $a = 2 \cdot 10^{-4}$ versus $1/\sqrt{\tau}$. A straight line is a good approximation to the results of the simulations.

A least-squares-fit of the curve in Fig. 5 to a straight line for $0.0 < 1/\sqrt{\tau} < 0.15$ give

$$\theta_2(\tau) = (0.546 \pm 0.002) - (0.236 \pm 0.007) \cdot 1/\sqrt{\tau} \tag{14}$$

[2] All results discussed from here on are based on these 35 configurations.

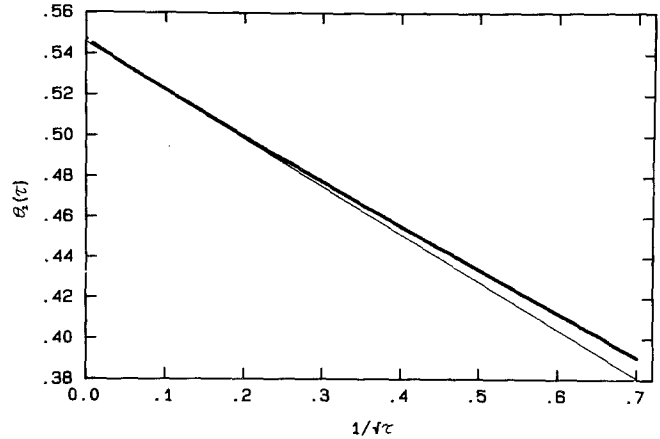

Fig. 5. The upper curve is the $1/\sqrt{\tau}$ behavior of the simulated surface coverage $\theta_2(\tau)$. The lower curve is a straight line resulting from a least-squares-fit of the data for $1/\sqrt{\tau} < 0.15$.

with an average rms deviation of 0.0004 per point. From this we get an extrapolated value of the coverage at $\tau = \infty$, $\theta_2(\infty) = 0.546 \pm 0.002$. This is within the uncertainty of the value obtained above.

In Fig. 5 we see the same slow convergence as in the one-dimensional case in Fig. 2, but now in units of $1/\sqrt{\tau}$ instead of $1/\tau$. In these units of time the approach toward the asymptotic limit is approximately the same.

In the next section we introduce the concept of circular holes and define the hole-size distribution function $P(d_h)$—the analog of the one-dimensional function $p(x)$ in eq. (7). At the cutoff value where the hole diameter d_h equals the disk diameter d, we find $P(d_h = d) = 0.432 \pm 0.02$. Noticing that $\theta_2(\infty) \cdot P(d_h = d) = 0.236 \pm 0.01$, we see from eq. (14) that within our numerical error we can write

$$\theta_2(\infty) - \theta_2(\tau) = \theta_2(\infty)\, P(d_h = d) \cdot 1/\sqrt{\tau} + \cdots \tag{15}$$

In Appendix A we show that the surface saturates as

$$\theta_D(\infty) - \theta_D(\tau) = \frac{T_D}{D} K_D \theta_D(\infty)\, P(d_h = d) \cdot \tau^{-1/D} + \cdots \tag{16}$$

The topological number T_D is explained in Appendix B. It is defined as the number of vertices per cell in a D-dimensional VD network. $T_1 = 1$, $T_2 = 2$, and $T_3 \cong 6$. K_D is a geometrical constant we have not been able to evaluate except for one dimension where $K_1 = 1$. Comparing eqs. (15) and (16) seems to suggest also that $K_2 = 1$. It is then tempting to speculate that this is generally the case.

We finish this section with a few comments on the geometrical properties of the RSA configuration. Consider the RSA configuration in Fig. 4. Most observers tend to see texture, clusters, strings, and structures, and most tend to insist that the packing is not completely jammed. The quantitative measures easily generated for random packing geometries are density, specific surface, and the statistical distributions of local properties. These properties are not easily appreciated by just looking at the figure. In fact the eye seems to see structure on a different scale involving correlations of many particles. If we increase the disk radius slightly in a configuration like that in Fig. 4, we can define a cluster as a set of overlapping disks. For an increase of radius by 20% the biggest cluster will percolate through the sample and look like Fig. 6. The cluster connectivity depend of course on the increase of radius. For the RSA configuration the percolating cluster will show up for the first time when the radius is increased by nearly 20%, an unexpected high value. The cluster size as a function of disk radius, their scaling properties, and so on represent a percolation problem useful in characterizing a random geometry like that in Fig. 4. We may also ask the

Fig. 6. The percolating cluster of disks generated by increasing the disk radii in Fig. 4 by 20%.

same questions about the void between the disks. In two dimensions the void stops percolating when the disks starts to percolate. We pursue these aspects of the RSA configurations in a later paper.

4. PORES OR HOLES IN THE JAMMED CONFIGURATION

In porous media and other random structures the pore-size distribution plays a central role and is used in models for the transport properties. It is not possible, however, to give an unambiguous general definition of what we mean by a pore. We chose to characterize pores through the definition of *circular holes*. A hole in a configuration of disks is defined by the following procedure: For any three disks under consideration we find the diameter d_h and the center of the circle that just touches these three disks. If this circle does not overlap any disk it is a hole. Note that by this definition, holes may overlap—and several overlapping holes combine to cover the intuitive pore.

Nonoverlapping holes can be defined in this way: By starting with a configuration of *overlapping holes*, we eliminate the holes overlapping the largest hole. Then we delete all holes overlapping the next largest hole of the remaining ones, and so on.

As explained in Appendix B, there are exactly two overlapping holes per disk. We therefore introduce the normalized probability density per

pair of disks of fiding overlapping (nonoverlapping) holes with a diameter in an infinitesimal interval around d_h, which is plotted in Figs. 7 and 8. The lower cutoff value is given by the smallest hole that can be defined by three disks with three points in contact; $d_0/d = (\sin \pi/3)^{-1} = 0.155$; see Fig. 9. The upper cutoff is due to the definition of the jamming limit. If the hole

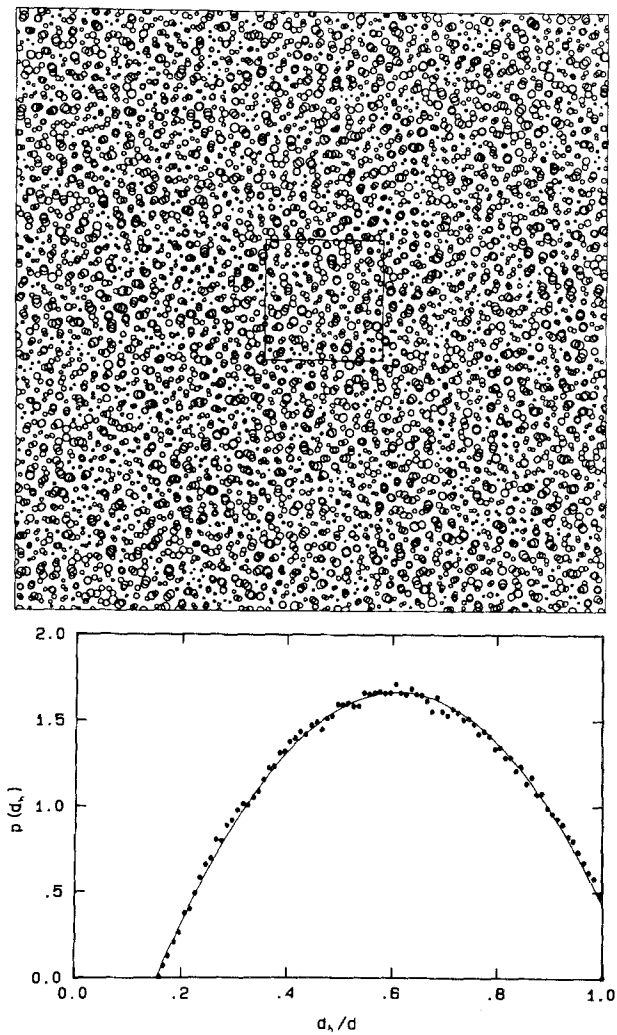

Fig. 7. The top figure shows the overlapping holes for the configuration in Fig. 4. (The central square is magnified in Fig. 14.) The lower figure is the size distribution of overlapping holes at the jamming limit for the RSA configuration: d_h is the hole diameter and d is the disk diameter. The solid curve is a fitted parabola.

diameter d_h is bigger than the disk diameter d, then the jammed configuration is not reached. This was in fact the situation after 10^8 trials. On the average we found nine holes bigger than a disk in or simulations, and about 10% of our replicas had overlap between two of these holes at this stage in the simulations. By locating these holes and placing disks into them, we reached the jamming limit described in Section 3. The hole-size distribution contains information about the local disk configuration.

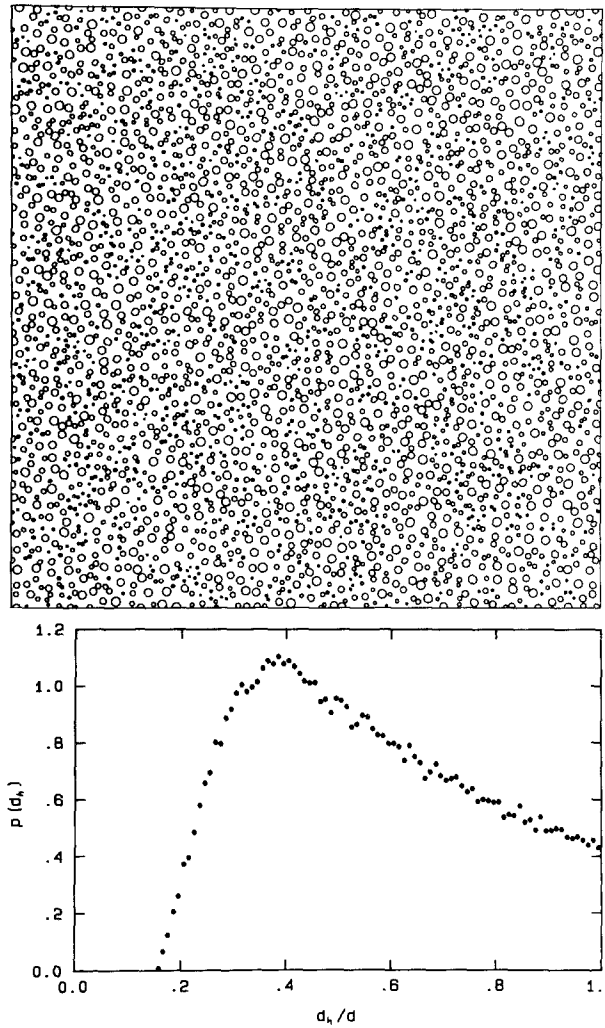

Fig. 8. The top figure shows the nonoverlapping holes generated from the overlapping holes in Fig. 7. The bottom figure is the size distribution of the nonoverlapping holes of the RSA configuration at the jamming limit.

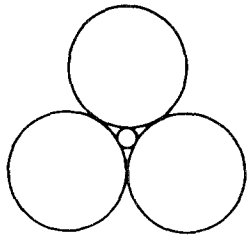

Fig. 9. The smallest hole is defined by three disks with three points in contact: $d_0/d = (\sin \pi/3)^{-1} - 1 = 0.155$.

The distribution of the overlapping holes is well-described by the parabola

$$P(d_h/d) = (b_1/d^2)(d_h - d_0)(b_2 - d_h) \tag{17}$$

where $b_1 = 8.08 \pm 0.05$ and $b_2/d = 1.063 \pm 0.003$, as shown in Fig. 7. We have not yet found a good theoretical explanation for this result. The limiting value for $d_h = d$ is $P(1) = 0.432 \pm 0.02$. This value is close to the one-dimensional value 0.4217 obtained in eq. (9), and one might speculate that these limiting values are the same.

The average number of overlapping holes in the RSA configuration is 5465 ± 29, and we have two overlapping holes per disk. As shown in Appendix B, the overlapping holes are directly related to the corners of the Voronoi–Dirichlet tessellation. This connection leads to the topological constraint that for any random disk packing the number of holes per disk is exactly 2.

The total area of the overlapping holes is $A_{OH} = 0.439 \pm 0.004$. The mean relative area of an overlapping hole is then $8.034 \cdot 10^{-5}$, giving a mean hole diameter $d_h/d = 0.63$. This value is very close to the maximum of the distribution in Fig. 7.

The distribution of the nonoverlapping holes consists of two parts with a change in behavior due to the decimation of overlapping holes around the most probable value $d_h/d = 0.4$. Holes with diameter $d_h/d < (\sqrt{17} - 3)/4 = 0.2808$ cannot overlap any other hole and thus are unaffected by the decimation procedure. Thus the initial part of the distribution follows the parabola in Fig. 7. The reason why the distributions in Figs. 7 and 8 have nearly the same limiting value at $d_h/d = 1$ is due to our procedure of making the nonoverlapping holes.

The nonoverlapping holes have a mean area of $A_{NOH} = 0.231 \pm 0.002$, and there are 1.2 nonoverlapping holes perdisk. The mean relative area of a nonoverlapping hole is $7.039 \cdot 10^{-5}$, giving a mean-hole diameter of $d_h/d = 0.59$. This is nearly the same mean as for the overlapping holes, but

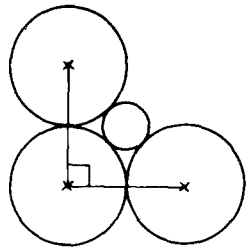

Fig. 10. The largest hole defined by three disks with two points in contact, or the smallest unstable hole: $d_h/d = (\sin \pi/4)^{-1} - 1 = 0.414$.

it is considerably different from the most probable value in Fig. 8. The largest hole defined by three disks with two points in contact—Fig. 10—has a diameter $d_h/d = (\sin \pi/4)^{-1} - 1 = 0.414$. This value is very close to the most probable value of the nonoverlapping holes.

The hole shown in Fig. 10 is on the borderline between what we call *stable* and *unstable* holes. If a hole has its center inside the triangle defined by the centers of the disks defining the hole, it is *stable*; otherwise it is *unstable*. A hole is stable in the sense that a translation of the hole will result in overlap with disks unless the hole diameter is reduced. We expect the notion of stable holes to be important in multiphase fluid displacement in porous media where surface tension effects tend to trap one phase in the pores.

The size distributions of stable holes are shown in Fig. 11. The size distribution of the stable overlapping holes consists of two regions. Since any

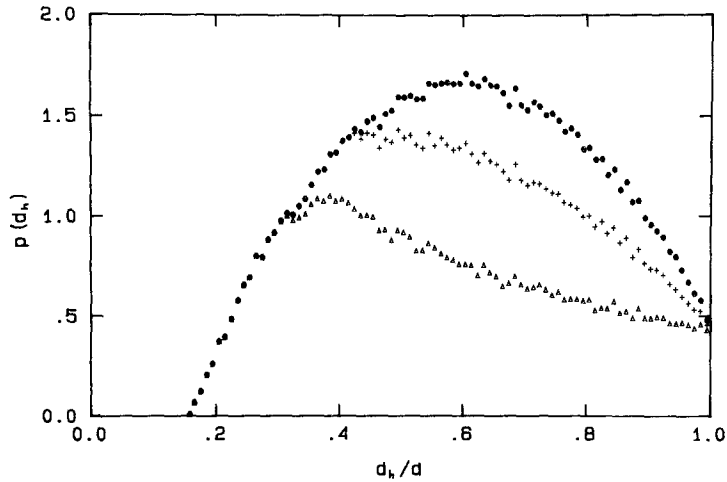

Fig. 11. Size-distribution of holes: ○, all overlapping holes. +, stable overlapping holes. △, stable nonoverlapping holes. This distribution is indistinguishable from that in Fig. 8.

hole smaller than $d_h/d=0.4$ is stable, they are not affected by the requirement of stability and thus the shape of the distribution for $d_h/d<0.4$ is unchanged.

Statistically we cannot distinguish the stable nonoverlapping holes from all the nonoverlapping holes. Thus our procedure of deleting overlapping holes in addition deletes most of the unstable holes in the RSA configuration. Also a local configuration similar to that in Fig. 10 has a high probability.

5. THE RADIAL DISTRIBUTION FUNCTION

The probability density $\rho(r)$ for finding another disk at a distance between r and $r+dr$, given a disk at the origin, is called the radial distribution function or the radial pair-correlation function. The radial distribution function is central in experimental applications of geometrical concepts to physical systems, since it defines the scattering function measured in light-, X ray-, and neutron-diffraction experiments. For point particles distributed randomly on a surface with an average number density of $\bar{n}$ particles per unit area, the radial distribution function follows directly from the fact that the expected number of particles in an annulus of area $2\pi r\,dr$ is just the area of the element times $\bar{n}$

$$\rho_{\text{ran}}(r)=2\pi r\bar{n} \tag{18}$$

We define the dimensionless pair-correlation function $G(r)$ for the RSA configuration by

$$G(r)=\rho(r)/\rho_{\text{ran}}(r) \tag{19}$$

which is normalized so that $G(r)\to 1$ when $r\to\infty$. In Fig. 12 we have plotted $G(r)$ for the RSA configuration. We see that $G(r)$ has a divergence at contact, and also that it is strongly damped so that the RSA configuration looks random (i.e., $G(r)=1$) for $r/d>2.5$.

The divergence of $G(r)$ at $r=d$ is logarithmic.[6-8] The insert in Fig. 12 shows $G(r)$ plotted against $\ln(r/d-1)$ for $r/d<1.3$. We do not see the asymptotic behavior over more than 1.5 decades due to the low statistics at small distances. A least-squares-fit in the range $1.008<r/d<1.18$ gives

$$G(r)=-(1.19\pm 0.1)\ln[(r/d)-1]+\cdots \tag{20}$$

The uncertainty is estimated by varying the range of the fit of r/d down to 1.0001.

In Appendix A we show that the general form of $G(r)$ is

$$G(r)=-\frac{(D+1)\,T_D}{D2^{D-1}}\frac{1}{\theta_D(\infty)}P(d_h=d)\ln[(r/d)-1]+\cdots \tag{21}$$

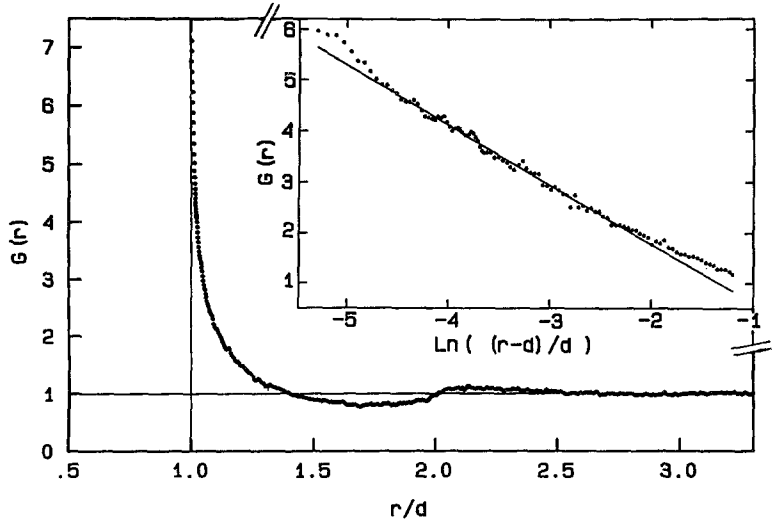

Fig. 12. The radial distribution function $G(r)$ for disks of diameter d as a function of disk separation r for RSA configurations at the jamming limit $\theta_2 = 0.547$. The insert shows a semilogarithmic plot of the divergence in the pair-correlation function near contact. The line is a least-squares-fit of the data points to a straight line.

where $P(d_h)$ is the hole-size distribution defined in the previous section. This equation is correct in one dimension, eqs. (9) and (12). From our two-dimensional simulations, eq. (21) gives $G(r) = (1.18 \pm 0.06) \ln(r/d - 1) + \cdots$, in good agreement with the result (20).

6. THE VORONOI–DIRICHLET DIVISION OF SPACE

To each disk configuration there is a conjugate Voronoi–Dirichlet (VD) division of space—see Figs. 13 and 14. This division is defined as follows. Around every disk center we find the set of points closer to this disk center than to any other disk center. These sets define the interior of convex polygons. By definition each VD cell contains one and only one disk. In a close packed configuration the VD tessellation consist of regular hexagons. In a random configuration we find different types of polygons. The statistics of these polygons is one of the few tools we have in characterizing a random geometry.

There are several topological constraints on a VD network, and therefore also on the disk configuration defining it. In two-dimensions these constraints are relatively strong. In Appendix B we show that topology requires the average number of edges per polygon to be precisely six for any network in which three edges meet at a corner. In Table II we have

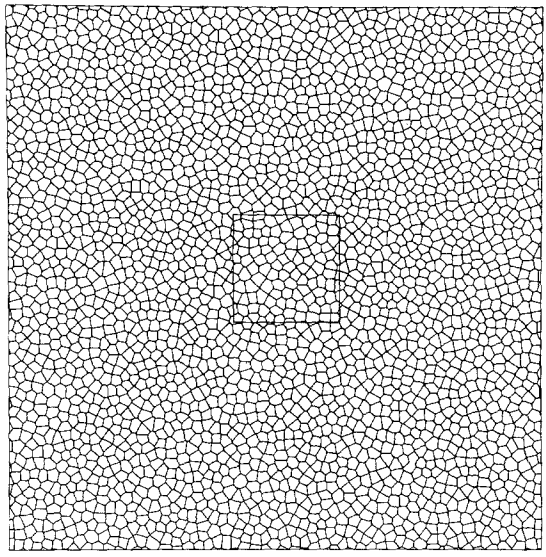

Fig. 13. The figure shows a VD division of space for the RSA configuration in Fig. 4. (The central square is magnified in Fig. 14.)

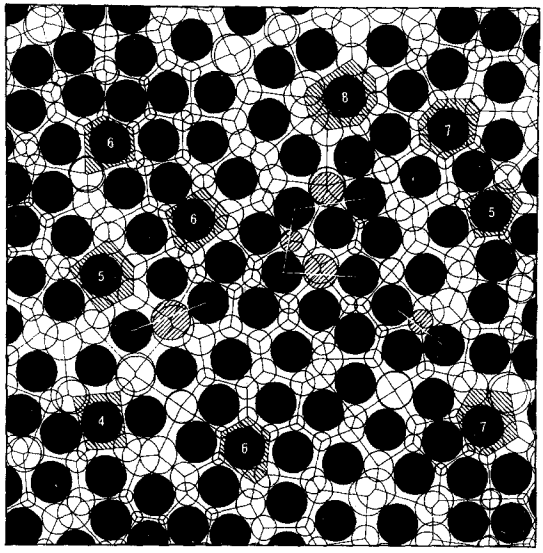

Fig. 14. A magnification of the central part in Figs. 4, 7, and 13 showing the connection between overlapping holes and VD vertices. Some indirect neighbor pairs are shown and the corresponding unstable holes are hatched. The numbers are the number of edges on the hatched polygons.

Table II. The Frequencies of VD Polygons Occurring in the RSA Configuration.

No. of edges	%
3	0.0
4	1.115
5	24.428
6	50.413
7	21.598
8	2.396
9	0.048
10	0.001
11	0.0
Total	99.999

summarized the frequencies of the different VD polygons occurring in the RSA configuration. We see that only 50% of the cells have 6 edges, but the average number of edges is 5.999. Some of these different polygons are hatched in Fig. 14.

In Fig. 15 we have plotted the distribution function for the area, the circumference, the side length, and the vertex angles of the VD polygons of

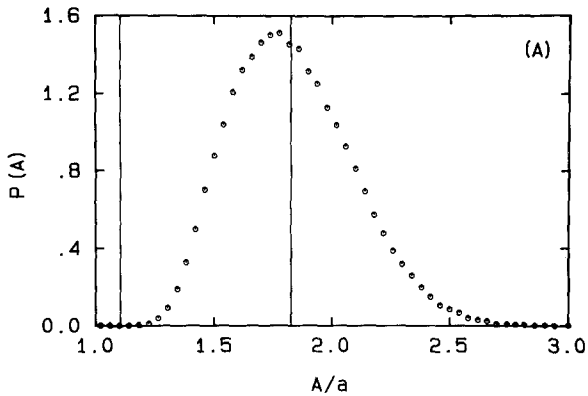

Fig. 15. Distributions functions for the VD polygons for the RSA configuration. The left vertical line is the δ-function peak in the corresponding distribution for a triangular close-packed structure and the right line is the corresponding peak for a triangular lattice at a coverage $\theta = \theta_2(\infty)$. (a) Distribution of polygon area A normalized with the disk area a. (b) Distribution of polygon circumference O normalized with the disk circumference $o = \pi d$. (c) Distribution of polygon sides L normalized with the disk diameter d. (d) Distribution of polygon angles φ.

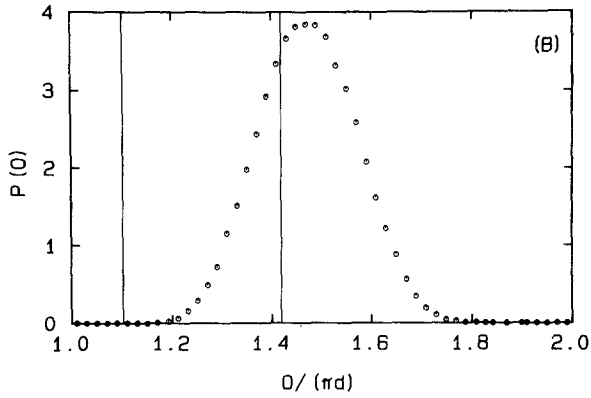

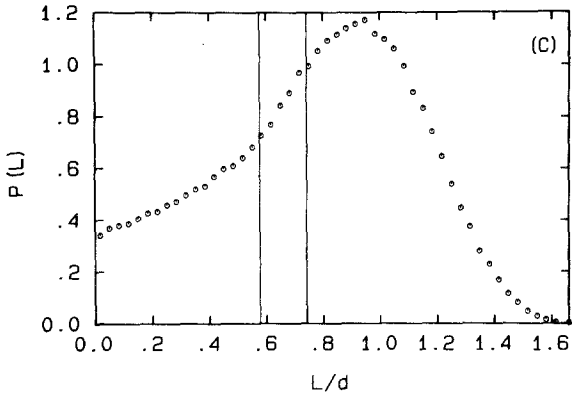

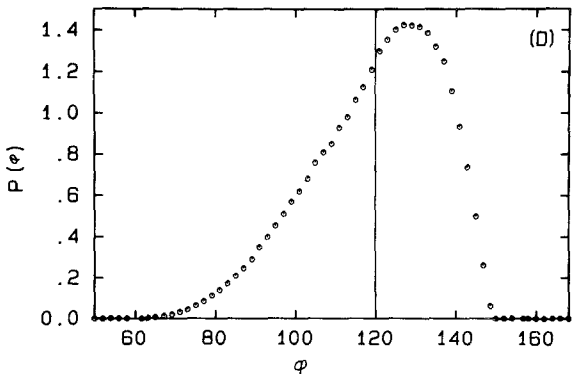

Fig. 15 (*continued*)

the RSA configurations. The left vertical straight line in these figures is the place of the δ-function peak in the corresponding distribution for a close-packed configuration. The right vertical straight line is the position of the δ-function peaks for a triangular lattice at the same coverage $\theta = 0.547$ as the RSA configuration. Of course, for the angle distribution these two δ-function peaks coalesce. All distributions in this section are probability densities normalized so that the total area under each curve is equal to unity.

The VD froth can be used to define what we mean by neighboring disks. Those disks that share a common side in the respective VD polygons, are called *geometrical neighbors* or a *contiguous pair.*[18] The number of geometrical neighbors—the *contiguity number*[18]—is the analog of the *coordination number* in a crystalline structure. Notice that this definition of a neighbor does not always give the nearest neighbor as a result for a crystalline arrangement. In Fig. 16 we show the probability distributions for finding the nth geometrical neighbor disk a distance x/d away from a given disk (for $n = 1$–6). All these six distributions would collapse in to a single δ-function peak for a triangular lattice. The probability distribution for the 5th and 6th nearest geometrical neighbors are derived from those disks with a contiguity number greater or equal to 5 and 6, respectively. Since the jammed configuration is reached, all distributions must be zero for $x/d \geqslant 2$. If this had not been the case, one vertex would be at a distance greater than a disk radius from the three disks defining it, and then there would be room for one more disk. This is why the asymmetry of the distributions shifts from having a steep rise near $x/d = 1$ for the nearest neighbors toward having a steep fall near $x/d = 2$ for the 6th nearest geometrical neighbor (and an even steeper fall for the 7th and 8th neighbor not shown in Fig. 16). Notice that the distribution of finding the nearest geometrical neighbor a distance x/d away is not peaked but has a logarithmic divergence at contact as the insert in the top figure in Fig. 16 shows. This is not surprising since the correlation function (Fig. 12) has a logarithmic divergence at contact. The probability distributions of the second and third nearest of the geometrical neighbors start out with a value greater than zero. So the probability density of finding three disks in contact with the same disk is different from zero.

We can divide the neighbors that the VD polygons define into *direct* or *indirect neighbors*, depending on whether or not the line joining the neighboring disk centers intersects their common side. In the RSA configurations 89.9% of the neighbors are direct neighbors. As explained in Appendix B, there is *one overlapping hole at each VD vertex* and there is *a one-to-one correspondence between stable and unstable holes and direct and indirect neighbors.* This shows that our circular holes and the VD division

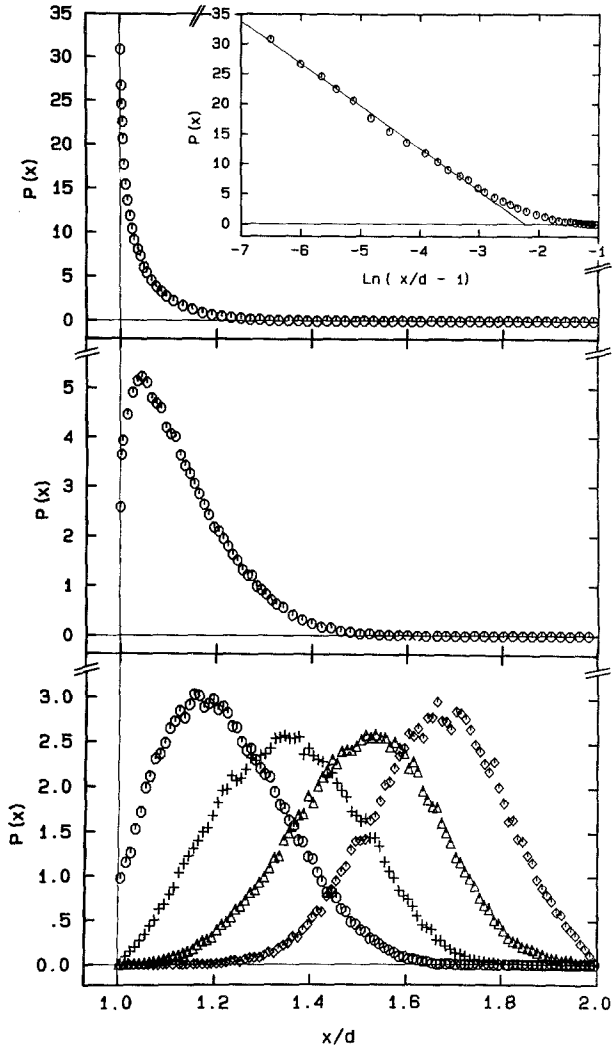

Fig. 16. Distance distribution to the geometrical neighbors of the RSA configuration. Top figure: The probability density of finding the closest geometrical neighbor a distance x/d away. The insert shows the distribution on a semilogarithmic plot for $x/d < 1.3$. Middle figure: The distance to the next-nearest geometrical neighbor disk. Lower figure: The distance to ○, 3rd neighbor disk; +, 4th neighbor disk; △, 5th neighbor disk; ◇, 6th neighbor disk.

of space are two aspects of the same thing. Both these correspondences are shown in Fig. 14. We believe that this identification may be of importance in understanding how flow properties are influenced by the pore-size distribution. If fluid flows in the space between the disks, the flow pattern is influenced by the pore necks or the distance between the direct neighboring disk pairs. With the identification we have established between direct neighbors and the stable holes, it may be possible to find out how the properties of the stable holes influence the flow pattern.

In Fig. 17 the probability density of finding the distance x/d between two disk centers defining an edge in a VD polygon, i.e., the distance between a geometrical neighbor pair, is plotted. This plot is in a sense the average of the distributions of neighboring disks in Fig. 16. Again we have a logarithmic divergence at zero resulting from the divergence of the pair-correlation function. Then the curve has a flat plateau before it changes behavior at $x/d \approx 1.65$. At this point it decreases more or less linearly until it reaches zero at $x/d = 2$. In the same figure we have also plotted the distance distribution between the direct neighbors only. This distribution do not have the same long flat plateau, but rather a small crossover region between a logarithmic behavior and a linear behavior.

In Fig. 18 we have plotted the distribution of the diameter x of the largest circle we can place in a VD polygon. This is a measure of the size of VD polygons and gives some additional information about the shape of the

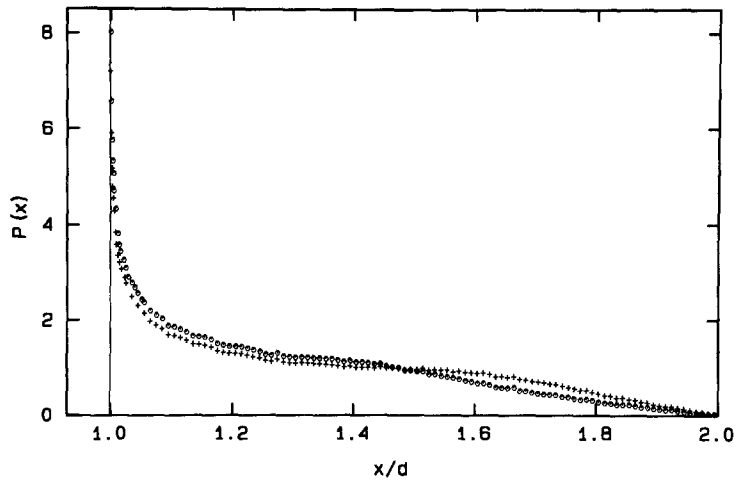

Fig. 17. +: the distance between two disks in a contiguous pair; ○: the distance between the direct geometrical neighboring disks only.

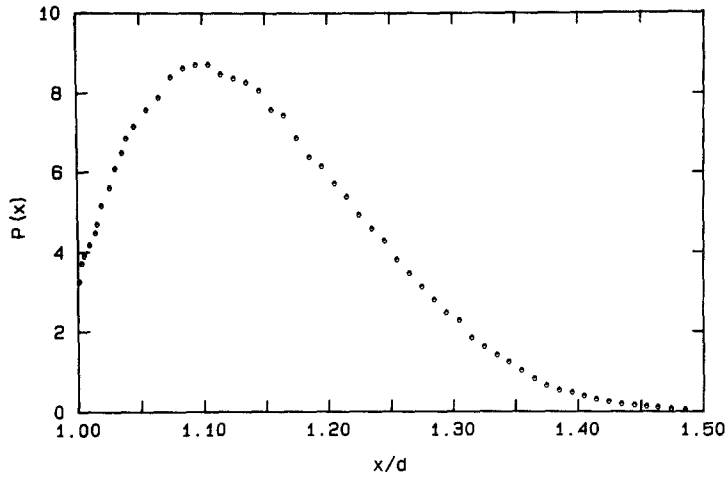

Fig. 18. The diameter of the largest inscribed circle in a VD polygon.

VD polygons. The rather large value at $x/d = 1$ implies that in many of the VD polygons the disk we have placed is in fact the largest we can place in that polygon.

7. SUMMARY

The main purpose of this paper was to investigate the geometrical properties of the two-dimensional RSA configuration. We simulated the one-dimensional problem to get an estimate of the computing accuracy in our two-dimensional simulations. In order to characterize the RSA configuration, we studied the statistical properties of the VD tessellation. To be able to give a pore-size distribution of the RSA configuration, we introduced the concept of circular holes. We identified the centers of these holes with the vertices of the VD network. This identification implies that the notion of stable/unstable holes are related to direct/indirect geometrical neighbors. The hole-size distribution for all overlapping holes was found to be a parabola. From our simulations we obtained a surface coverage at jamming in agreement with earlier works, and we found the correct asymptotic behavior of $\theta_2(\tau)$ and $G(r)$—first seen in simulations by Feder[6] and explained by Pomeau[7] and Swendsen.[8] In addition we found general relations for the amplitudes of the asymptotic behavior of $\theta_2(\tau)$ and $G(r)$. These relations connect the surface coverage, the radial distribution function, and the hole-size distribution function.

ACKNOWLEDGMENTS

We wish to thank Amnon Aharony and Erling Pytte for helpful comments on the manuscript. The financial support of Statoil is gratefully acknowledged.

APPENDIX A: ASYMPTOTIC BEHAVIOR OF $G(r)$ AND $\theta(\tau)$

Both the logarithmic divergence of the correlation function $G(r)$ and the asymptotic saturation of the surface coverage $\theta_D(\tau)$ were explained by Pomeau[7] and Swendsen.[8] Here we extend their arguments and obtain the rate of divergence of the correlation function, eq. (3) and the asymptotic form for the coverage, eq. (4). We now discuss $D=2$, and we compare our results with the exact $D=1$ results, but our results are valid in any dimension D.

Asymptotic Behavior of $\theta(\tau)$

If we draw a circle with radius twice the disk radius around a disk center, we obtain the area excluded by this disk. At time τ in the RSA process the area not excluded by any disk is the total target area for the center of the next disk to be adsorbed. In the beginning of the process the total target area will have a complex topology, but after a characteristic time $\tau^* \gg 1$, the target area will consist almost exclusively of simple isolated target areas of the type illustrated in Fig. 19 with room for only one disk

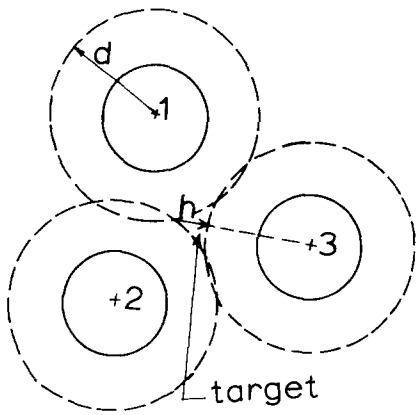

Fig. 19. Three disks defining a target area of size h in two dimensions.

each. In our $D=2$ simulations the characteristic time τ^* is of the order of 100. At this stage in the process most of the targets will be defined by three disks, as illustrated in Fig. 19, but there are also many small targets defined by four disks.

Let us look at the RSA process of placing disks of area a on a target area $\mathscr{A} \gg a$. Let the disks adsorbed in targets like the one in Fig. 19 with room for only one disk be colored red and the disks adsorbed in bigger targets be colored blue. Since each target is hit with a rate proportional to its area, the process of placing the blue disks will die out exponentially. So for times $\tau \gtrsim \tau^*$ most of the disks adsorbed are red. At time $\tau = \infty$ the jamming limit is reached and we have a configuration of red and blue disks with coverage $\theta_D = N_d a/\mathscr{A}$, where N_d is the total number of red and blue disks adsorbed. The total number of red disks only we call N_{red}, and their contribution to the coverage is $\theta_{\text{red}} = N_{\text{red}} a/\mathscr{A}$. It is the contribution from these red disks to the correlation function that gives rise to the logarithmic divergence, as we see in the next section.

First we describe the asymptotic behavior at large times of the coverage $\theta_D(\tau)$ in the RSA process. We therefore invent a process that focuses directly on this asymptotic behavior. Imagine that we remove all the red disks from our jammed configuration. We are then left with a configuration consisting of only isolated targets like the one shown in Fig. 19. The time τ is reset to zero and we study the RSA process of adsorbing (the red) disks starting with this initial configuration. This process will behave as the asymptotic behavior in the real RSA process.

A target in this initial configuration will be characterized by a length scale h and a set of angles Φ. The area of such a target can be written in the form

$$v = h^D f_D(\Phi) \tag{22}$$

Let $n_t(v;\tau)$ be the number density of targets with area in the range $(v, v+dv)$ at time τ in this process. Clearly $N_{\text{red}} = \int dv\, n_t(v;\tau=0)$. We throw disks at a constant rate, and with the definition of the time scale used the number of attempts to place a disk is $i = \tau\mathscr{A}/a$. The adsorption process satisfies the equation

$$(d/d\tau)\, n_t(v;\tau) = -(v/a)\, n_t(v;\tau) \tag{23}$$

with the solution

$$n_t(v;\tau) = n_t(v;\tau=0)\, e^{-v\tau/a} \tag{24}$$

At $\tau = 0$, the probability of finding a target with a length scale in the interval $(h, h+dh)$ and the angles in $(\Phi, \Phi+d\Phi)$ is $dh\, d\Phi\, P(h, \Phi)$. The

probability of finding a target of volume v in the range $(v, v+dv)$ is therefore given by eq. (22)

$$dv\, P(v) = dv \frac{1}{D} v^{(1/D)-1} \int d\Phi\, f_D^{-1/D}(\Phi)\, P(h, \Phi) \tag{25}$$

Since the disks are placed at random on the surface with uniformity in any given direction, the probability $P(h, \Phi)$ must be smooth at $h=0$. The targets we focus on are so small that we can write

$$P(v) = (1/D)\, v^{(1/D)-1} (1/d)\, A_D \tag{26}$$

where we have introduced a dimensionless geometrical quantity

$$A_D = d \int d\Phi\, f_D^{-1/D}(\Phi)\, P(h=0, \Phi) \tag{27}$$

d is the disk diameter. By use of eq. (24) we find the total number of holes at time τ is

$$N_t(\tau) = \int_0^{v_{\max}} dv\, N_{\text{red}} P(v)\, e^{-v\tau/a} \tag{28}$$

Because of the exponential decay we may take the upper limit to infinity with a small error. If we insert eq. (26) we obtain

$$N_t(\tau) = N_{\text{red}}(1/D)\, \Gamma(1/D)(1/d)\, A_D (\tau/a)^{-1/D} \tag{29}$$

where Γ is the gamma function, so that $\Gamma(1/D) = \sqrt{\pi}$ for $D=2$. For each target that gets occupied, the coverage will increase with $a/\mathscr{A}$. Thus the coverage is given by

$$\begin{aligned} \theta_D(\infty) - \theta_D(\tau) &= \frac{a}{\mathscr{A}} N_t(\tau) \\ &= \frac{1}{D} \frac{\sqrt{\pi}}{2} \left[\Gamma\left(\frac{D}{2}+1\right) \right]^{-1/D} \Gamma\left(\frac{1}{D}\right) \theta_{\text{red}} A_D \tau^{-1/D} \end{aligned} \tag{30}$$

where we have made use of the fact that

$$a^{1/D} = \frac{\sqrt{\pi}}{2} \left[\Gamma\left(\frac{D}{2}+1\right) \right]^{-1/D} d \tag{31}$$

Equation (30) is the correct asymptotic behavior of the RSA process. In one dimension where we do not have any angles, we get

$$\theta_1(\infty) - \theta_1(\tau) = d\theta_{\text{red}} P(h=0)\, 1/\tau \tag{32}$$

where d is now the length of one line segment. Comparing this result with the exact asymptotic results in eq. (10) we see that

$$d\theta_{\text{red}} P(h=0) = e^{-2\gamma} = d\theta_1(\infty)\, p(x=d) \tag{33}$$

We explain this identification in the next section.

Asymptotic Behavior of $G(r)$

Consider the radial correlation function $G(r)$ defined in Section 5. If a disk is placed on a target (h, Φ) as illustrated in Fig. 20, it will make $D+1=3$ contributions to $G(r)$; but, averaged over all targets, we get the same contribution from each of disks 1, 2, and 3. We therefore focus on the contribution from just one of the disks, say 3. Let $P(z \mid h, \Phi)\, dz$ be the probability that a new disk center is placed in a range dz at a distance $d+z$ from disk 3, given that disks 1, 2, and 3 define a target (h, Φ). We now approximate the target simplex in Fig. 20 by a triangle with height h and base angles $\Phi = (\varphi_1, \varphi_2)$; see Fig. 21. In the random sequential adsorption process disks are placed at random and the position of a new disk over any given interval is uniformly distributed. Therefore, the probability that a disk is placed in the area element dA defined in Fig. 21 is given by

$$dA = (h-z)\, g(\Phi)\, dz \tag{34}$$

where

$$g(\Phi) = \left[\frac{1}{\tan\varphi_1} + \frac{1}{\tan\varphi_2}\right] \tag{35}$$

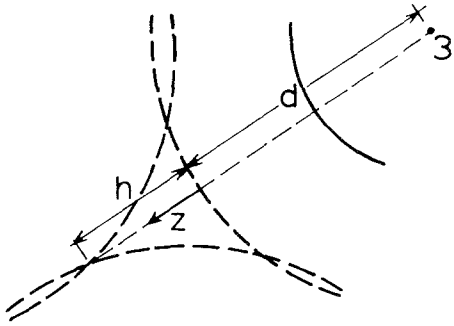

Fig. 20. The target area defined by the disks 1, 2, and 3 in Fig. 19, enlarged. To calculate the radial correlation function $G(d+z)$, we must first find the conditional probability that a disk is placed a distance $d+z$ from disk 3.

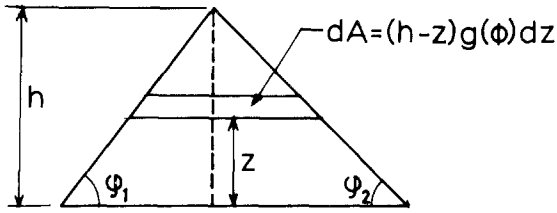

Fig. 21. The target (h, Φ) in Fig. 20 is approximated by a triangle with height h and base angles φ_1 and φ_2.

Consequently we find that the probability density $P(z\,|\,h, \Phi)$ is given by

$$P(z\,|\,h, \Phi) \sim (h-z)\, g(\Phi) \tag{36}$$

Since exactly one disk is placed on the target before the jamming limit is reached, we have the normalization condition

$$1 = \int_0^h dz\, P(z\,|\,h, \Phi) \tag{37}$$

This condition with eq. (36) then gives the explicit form for the conditional probability density

$$P(z\,|\,h, \Phi) = Dh^{-D}(h-z)^{D-1} \tag{38}$$

Although derived for $D=2$, this expression is also valid for any dimension D. Note that the angle-dependent part $g(\Phi)$ has dropped out of the final expression.

The change in the radial distribution function obtained by adding all the red disks to the configuration of blue disks is

$$\Delta\rho(d+z) = \frac{2}{N_d}(D+1)\int_z^{h_{\max}} dh\, d\Phi\, P(z\,|\,h, \Phi)\, P(h, \Phi)\, N_{\text{red}} \tag{39}$$

Factor 2 is due to the fact that if we measure the radial distribution function by placing each disk at the origin and then count the number of times we find another disk a distance $d+z$ from the origin, we will count every occurrence twice. The denominator N_d is the total number of measurements done. Also in this equation we make use of the fact that $P(h, \Phi) \approx P(h=0, \Phi)$.

The dimensionless correlation function $G(d+z)$ defined in eq. (19) is changed by

$$\Delta G(d+z) = \frac{\Delta\rho(d+z)}{\Omega_D (d+z)^{D-1}\bar{n}} \tag{40}$$

In this equation Ω_D is the total solid angle in D dimensions and $\bar{n} = N_d/\mathscr{A}$ is the number density of particles. From eqs. (38) and (39) we see the origin of the divergence in $\Delta G(d+z)$. The leading behavior (and the exact behavior in $D=1$) for the probability of placing disks in the interval dz a distance $d+z$ from the origin, is inversely proportional to the size h of the target. Therefore, the leading contributions to $\Delta G(d+z)$ for a given z are from the smallest possible targets bigger than z.

We can now express the full correlation function $G(d+z)$ as $G(d+z) = \Delta G(d+z) + (\textit{regular part})$. Inserting eq. (38) in (39) and focusing on the lower limit in the integration for small z, we finally get

$$G(d+z) = -\frac{D+1}{2^{D-1}\theta_D^2}\,\theta_{\text{red}}\,B_D \ln\frac{z}{d} + \cdots \tag{41}$$

$B_D = d\int d\Phi\, P(h=0, \Phi)$ is a new dimensionless geometrical quantity. Equation (41) is verified by the results of our simulations in Fig. 12.

In one dimension, we can compare eq. (41) with the exact expression for the asymptotic limit in eq. (12) and again recover eq. (33). Our asymptotic arguments are therefore consistent with the exact one-dimensional results.

Both rates in eqs. (30) and (41) depend on the arbitrary definition of red and blue disks. If we color all disks placed in a triangular target with a scale less than h red and the rest blue, we can choose the scale h arbitrary. The correct asymptotic rates cannot have this arbitrariness. We therefore want to find expressions that are exact. We define $p_{\text{blue}}(d+x)$ as the probability density of finding a circular hole with diameter $d+x$. Each hole is centered on a vertex of the VD network, and there are T_D vertices per disk. Since a hole bigger than a disk in the blue configuration is also a target area for a red disk, we must have that

$$T_D N_{\text{blue}}\, p_{\text{blue}}(d+h) = N_{\text{red}} \int d\Phi\, P(h, \Phi) \tag{42}$$

The asymptotic behavior comes from the limit $h \to 0$. We may therefore take this limit in the definition of the red disks. This means that $N_{\text{red}} \to 0$ or $N_{\text{blue}} \to N_d$ in such a way that eq. (42) still holds. In the asymptotic limit we must have $\theta_{\text{red}} B_D = \theta_D\, dp(d_h = d)$, where $dp(d_h) = P(d_h)$ is the hole-size distribution for the jammed configuration defined in Section 4. The correct rate for the correlation function is therefore

$$G(d+z) = -\frac{(D+1)\,T_D}{D2^{D-1}\theta_D}\, dp(d_h = d) \ln\frac{z}{d} + \cdots \tag{43}$$

The rate of saturation can be written

$$\theta_D(\infty) - \theta_D(\tau) = (T_D/D)\,\theta_D(\infty)\,K_D\,dp(d_h = d)\,\tau^{-1/D} + \cdots \tag{44}$$

where K_D is a geometrical constant given by

$$K_D = \frac{\sqrt{\pi}}{2}\Gamma\left(\frac{1}{D}\right)\left[\Gamma\left(\frac{D}{2}+1\right)\right]^{-1/D}\frac{1}{p(d_h=d)}\int d\Phi\, f_D^{-1/D}(\Phi)\, p(d_h=d,\Phi)$$

$$= \Gamma\left(\frac{1}{D}\right)\frac{1}{dp(d_h=d)}\int d\Phi\left(\frac{a}{f_D(\Phi)}\right)^{1/D} p(d_h=d,\Phi) \tag{45}$$

$p(d_h, \Phi)$ is the angle-dependent, hole-size distribution for the jammed RSA configuration at its upper cutoff value. In one dimension, where we do not have any angle integration, $K_1 = 1$. This explains the identification in equation (33). In two dimensions our numerical simulations seem to suggest that $K_2 = 1$ also. We have not found an explanation for this fact yet.

APPENDIX B: TOPOLOGICAL CONSTRAINTS FOR A TESSELLATION

For the sake of completeness we discuss here some of the well-known topological constraints existing in a general tessellation of space, and find the value of the topological number T_D entering eqs. (3) and (4) in two and three dimensions. T_D is defined as the number of vertices per disk in a VD network. In one dimension T_1 is trivially 1. At the end of this appendix we make a comment on the new result that the VD vertices and holes are closely related.

The starting point for the discussion is a theorem by Euler called the Euler–Poincaré theorem. In two dimensions this theorem states that

$$V - E + F = 1 \tag{46}$$

V is the number of vertices in a general division of space, E is the number of edges or links, and F is the number of faces. Equation (46) is true for any polygon assembly in two dimensions. In our case, the number of faces equals the number of disks in a configuration. The proof of this equation is simple in two dimensions. Following Coxeter,[19] we start with a graph consisting of one vertex only. From this starting point we want to construct any given connected polygon assembly. In Fig. 22 we show the only two possibilities that can occur in this construction. Either we can include a new vertex, thus creating a new edge also, or we can put an edge between

Fig. 22. The two different steps in constructing a tessellation.

two already existing vertices, giving a new edge and a new face. In both cases we see that $V-E+F=constant$. The constant in this expression is given from the initial condition with one vertex and depends on the topology of the space. On a sphere it is 2, on a plane it is 1, and on a torus it is 0.

It is also easy to see that a vertex where four edges meet splits into two vertices with three edges meeting, as indicated in Fig. 23 by an infinitesimal shift of the disks defining the VD vertex. In any random array without any special symmetry, the situation where four edges meet is therefore extremely rare. We thus conclude that exactly three edges meet in a vertex. Since each edge has two endpoints, it follows that

$$3V=2E \tag{47}$$

for all two-dimensional configurations without any special symmetry. Using eqs. (46) and (47) and the fact that $F\gg 1$ for a big system, we obtain

$$\begin{aligned} V &\approx 2F \\ E &\approx 3F \end{aligned} \tag{48}$$

i.e., there are two vertices for each face or disk, and there are three edges or links for each disk. This also shows that in two dimension, the topological

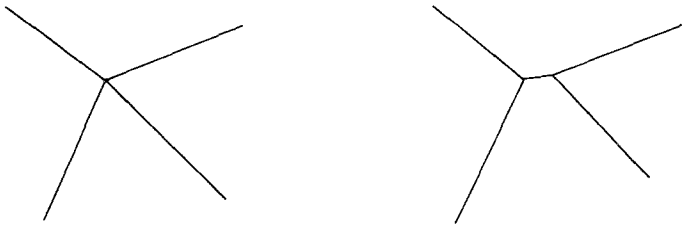

Fig. 23. A vertex where four edges meet splits up in two vertices where three edges meet by an infinitesimal change in the disk configuration.

number $T_2 = 2$. We now let F_p denote the number of faces with p sides. Since each edge is shared by two neighboring polygons and since there are pF_p edges belonging to polygons with p sides, we have

$$E = \frac{1}{2} \sum_p pF_p \tag{49}$$

Inserting eqs. (47) and (49) in eq. (46) and making use of the fact that $F = \sum_p F_p$, gives

$$\frac{1}{3} \sum_p pF_p - \frac{1}{2} \sum_p pF_p + \sum_p F_p = 1 \tag{50}$$

From this equation we get a topological constraint for these configurations

$$\bar{p} \equiv \frac{\sum_p pF_p}{\sum_p F_p} = 6 \tag{51}$$

or, in other words, that the mean number of edges of a polygon is 6.

To find T_3 we must start with a generalization of eq. (46)[18]

$$V - E + F - C = 1 \tag{52}$$

V, E, and F have the same meaning as before, but C is the number of cells—three-dimensional objects. By similar reasoning that led to eq. (47), one obtains the relations among these numbers for a random network in three dimensions[18]

$$6V = 3E = \bar{p}F = (\bar{f}\bar{p}/2)C \tag{53}$$

Here $\bar{p}$ is the average number of edges per face and $\bar{f}$ is the average number of faces per cell. Using the relations in eq. (53) in eq. (52), solving for $\bar{f}$ in terms of $\bar{p}$ gives

$$\bar{f} = \frac{12}{6 - \bar{p}} \tag{54}$$

This is a topological constraint in three dimensions and we see that it is much weaker than the one in two dimensions—eq. (51). From eqs. (53) and (54) we see that

$$T_3 = \frac{\bar{p}}{6 - \bar{p}} \tag{55}$$

Empirically, Finney[17] found the value $\bar{p} = 5.158 \pm 0.002$ for a random close-packed configuration. Theoretical models of Coxeter[19] for the ran-

dom close-packed configuration yields values close to this experimental value. If we assume that this value is the same for the RSA configuration, the topological number $T_3 \approx 6$. But two random configurations in three dimensions need not have the same average number of sides per face, as long as eq. (54) is fulfilled.

Our last remark concerns the property we found in Section 4, namely that there are exactly two holes per disk in a random configuration. The property that a hole center is equidistant from three disks, and that the hole is not allowed to overlap any disk—such that the distance to any other disk from the hole center is greater—implies that every overlapping hole is a Voronoi–Dirichlet vertex and vice versa. Therefore, a hole configuration and a VD tessellation are closely related. From eq. (48) we then see that $V \approx 2F$ means that there are exactly two overlapping holes for each disk in a configuration.

REFERENCES

1. J. J. González, P. C. Hemmer, and J. S. Høye, *Chem. Phys.* **3**:228 (1974).
2. L. Finegold and J. T. Donnell, *Nature* **278**:443 (1979).
3. M. Hasegawa and M. Tanemura, in *Recent Developments in Statistical Interference and Data Analysis*, K. Matusita, ed. (North-Holland, Amsterdam, 1980).
4. J. Feder and I. Giaever, *J. Coll. Interface Sci.* **78**:144 (1980).
5. B. Widom, *J. Chem. Phys.* **44**:3888 (1966).
6. J. Feder, *J. Theor. Biol.* **87**:237 (1980).
7. Y. Pomeau, *J. Phys. A: Math. Gen.* **A13**:L193 (1980).
8. R. H. Swendsen, *Phys. Rev. A* **24**:504 (1981).
9. A. Renyi, *Publ. Math. Inst. Hungar. Acad. Sci.* **3**:109 (1958). English Translation: *Sel. Trans. Math. Stat. Prob.* **4**:203 (1963).
10. J. K. Mackenzie, *J. Chem. Phys.* **37**:723 (1962).
11. B. Widom, *J. Chem. Phys.* **58**:4043 (1973).
12. B. E. Blaisdell and H. Solomon, *J. Appl. Prob.* **7**:667 (1970).
13. W. S. Jodrey and T. M. Tory, *J. Statist. Comput. Simul.* **10**:87 (1980).
14. E. M. Tory, W. S. Jodrey, and D. K. Pickard, *J. Theor. Biol.* **102**:439 (1983).
15. M. Tanemura, *Ann. Inst. Stat. Math.* **31B**:351 (1979).
16. J. D. Bernal, *Proc. Roy. Soc. Lond.* **A280**:299 (1964).
17. J. L. Finney, *Proc. Roy. Soc. Lond.* **A319**:479 (1970).
18. R. Zallen, *The Physics of Amorphous Solids* (John Wiley & Sons, New York, 1983).
19. H. S. M. Coxeter, *Introduction to Geometry*, 2nd ed. (John Wiley & Sons, Toronto, 1969).